symmetry

MDPI

Article

Experimental Design for Testing Local Lorentz Invariance Violations in Gravity

Ya-Fen Chen, Yu-Jie Tan and Cheng-Gang Shao *

Key Laboratory of Fundamental Physical Quantities Measurement of Ministry of Education, Hubei Key Laboratory of Gravitation and Quantum Physics, School of Physics, Huazhong University of Science and Technology, Wuhan 430074, China; chenyafen@hust.edu.cn (Y.-F.C.); yjtan@hust.edu.cn (Y.-J.T.)
* Correspondence: cgshao@hust.edu.cn; Tel.: +86-138-7140-3311

Received: 19 September 2017; Accepted: 3 October 2017; Published: 10 October 2017

Abstract: Local Lorentz invariance is an important component of General Relativity. Testing for Local Lorentz invariance can not only probe the foundation stone of General Relativity but also help to explore the unified theory for General Relativity and quantum mechanics. In this paper, we search the Local Lorentz invariance violation associated with operators of mass dimension $d = 6$ in the pure-gravity sector with short-range gravitational experiments. To enlarge the Local Lorentz invariance violation signal effectively, we design a new experiment in which the constraints of all fourteen violation coefficients may be improved by about one order of magnitude.

Keywords: Local Lorentz invariance violation; pendulum experiment; experimental design

1. Introduction

Local Lorentz Invariance (LLI), as a built-in element of General Relativity (GR) (for recent overviews for its centenary see, for example, [1,2]), denotes that the physical results are kept invariant when rotations and boosts are performed on a physical system. Though GR provides an impressive description of the wide variety of gravitational phenomena, a unified theory is expected to merge gravity and quantum physics, which is a very popular topic of current physics research [3]. However, current unified theories, such as string theory [4–6], predict that some modifications to the foundations of GR may induce some observable effects associated with the Lorentz violation. Thus, investigating the Lorentz violation is a worthy tool to test GR [7–14], and it may help us to explore the unified theory for GR and quantum mechanics.

In the past few years, LLI violation theories have developed rapidly, resulting in many frameworks to test LLI violation effects at attainable scales, such as the SME(Standard Model extension) frame [6,7], PPN (Parameterized post-Newtonian)frame [10,15,16], and so on. Here, we only focus on the testing Lorentz violation effect in the SME frame. In this frame, the LLI violating effect can be divided into three parts: a pure-matter sector, matter–gravity couplings and a pure-gravity sector, in which the last part can be written as a series with mass dimension d (such as $d = 4, 6 ...$). As experimental techniques are improved, combining theories and experiments to test LLI violation becomes an interesting work. Currently, the LLI violation effect for the pure-matter sector [17], matter–gravity couplings sector [8,18,19] and pure-gravity sector (for $d = 4$) have been widely studied. For the pure-matter sector, many experiments have been used to search for the LLI violation effect for different particles, such as photons, electrons, protons and so on. Here, take photon related experiments as a typical example, the available tightest photon-sector constraint currently is at 10^{-43} [20] for a certain particular operator. For LLI violation in matter–gravity couplings, the best current constraints are obtained at 10^{-11} GeV [19]. For LLI violation in the pure-gravity part, the experimental classification falls into three parts: experiments on ground [21], solar system [22], and astrophysical measurements [23,24], in which the different limits for different mass dimensions of LLI violation effects are given. For mass

dimension $d = 4$, the best constraints for violating coefficients are obtained at 10^{-12} [22] in solar system. In this paper, we focus on searching for LLI violation in pure-gravity sector for $d = 6$, which has been widely tested by short-range gravitational experiments, since the short-range experiments are better than other experiments to probe higher dimension coefficients with r-dependence. The best current limit for $d = 6$ is at 10^{-9} m^2 [25], which is given by a combined analysis for lab-based on-ground experiments HUST-2011 [26], HUST-2015 [27], IU-2002 and IU-2012 [28]. Based on the experiment performed in our lab, the test of the gravitational inverse square law, we have proposed a simple scheme to greatly enlarge the LLI violation signal [29]. Here, we will further refine the experimental part of the project.

This paper has the following structure: in Section 2, we will introduce the LLI violation coefficients in the SME frame expressed by the cartesian coefficients and Newton spherical coefficients, respectively. As the violating coefficients expressed in cartesian coefficients can be limited with the double trace condition, and each of the violation coefficients expressed by spherical decomposition can be independently limited. Thus, we shortly introduce the two types of expressions for the violating coefficients. In Section 3, the Lorentz violation torque in pendulum experiments is analyzed in detail. In Section 4, we introduce a new experimental design for testing the LLI violation effect with a stripe structure. Then it is followed by a simple discussion on it. Finally, we give a conclusion in Section 5.

2. LLI Violation in SME Frame

2.1. LLI Violation: Cartesian Coefficients

The Standard Model extension (SME) is an effective field theory describing Lorentz violation in low-energy experiments. The pure-gravity sector can be formulated as a Lagrange density composed of the usual Einstein-Hilbert term R and a cosmological constant, and the LLI violating terms expressed by an infinite series of operators with the increasing mass dimension d, which represents LLI violation [7,30],

$$L = \frac{\sqrt{-g}}{16\pi G_N}(R + \Lambda + L_M + L_{LV}^{(4)} + L_{LV}^{(5)} + L_{LV}^{(6)} + \cdots), \tag{1}$$

here, L_M is the matter term, and the last three terms are the Lorentz violation terms, which are constituted by the LLI violating coefficient field $k_{\alpha\beta\ldots}$ and the gravitationally physical quantities (curvature tensors $R_{\alpha\beta\gamma\sigma}$ [30] and its covariant derivatives). Here, we consider violating terms with $d = 6$, for which $L_{LV}^{(6)}$ can be written as:

$$L_{LV}^{(6)} = \frac{1}{2}(k_1^{(6)})_{\alpha\beta\gamma\delta\kappa\lambda}\{D^\kappa, D^\lambda\}R^{\alpha\beta\gamma\delta} + (k_2^{(6)})_{\alpha\beta\gamma\delta\kappa\lambda\mu\nu}R^{\kappa\lambda\mu\nu}R^{\alpha\beta\gamma\delta}. \tag{2}$$

which can be tested by gravity interaction at short range. In the Post-Newtonian approximation, Equation (2) results in the modified Poisson equation, and then the Lorentz violation potential between two masses in a lab frame can be written as

$$V_{\mathrm{LV}}(\vec{r}) = -Gm_1m_2\frac{\bar{k}(\hat{r})}{|\vec{r}^3|}, \tag{3}$$

in which the $\vec{r}$ is the vector separating two masses, the corrected factor $\bar{k}(\hat{r})$ is the background dynamical field via spontaneous Lorentz violation in lab frame, and it can be expressed as

$$\bar{k}(\hat{r}) = \frac{3}{2}(\bar{k}_{eff})_{iijj} - 9(\bar{k}_{eff})_{ijkk}\hat{r}^i\hat{r}^j + \frac{15}{2}(\bar{k}_{eff})_{ijkl}\hat{r}^i\hat{r}^j\hat{r}^k\hat{r}^l, \tag{4}$$

in which $\hat{r}^i$ is the projection of the unit vector along $\vec{r}$ in the ith direction, and the indices j, k, and l also stand for three spatial directions. For the lab-based, on ground experiments, as the LLI violating effect

is related to the rotation and boost of the Earth, it can be expressed by the tensor field of background in space-time. Besides, as the convention, the results of LLI violation coefficients from experimental searching are usually reported in the Sun-centered celestial-equatorial frame (SME frame). However, as the experiments take place on the earth, we should make a transformation for the LLI violation coefficients from lab frame to SME frame. Here, the lab frame (x, y, z) is defined as: the x axis is along the length direction of the pendulum and the angle of the x axis and local south is θ and the y and z axis point to east and the zenith, respectively. The SME frame (X, Y, Z) is defined as: the Z axis points along the direction of the Earth's rotation axis and the X axis points toward the vernal Equinox [31–35]. Thus, the LLI violating effect in the lab frame is modulated by the Earth's rotation, generating a sidereal torque signal experimentally [36]. Ignoring the Earth's boost (approximately to 10^{-4}), the SME frame (X, Y, Z) can be related to the lab frame (x, y, z) by a time-dependence rotation:

$$R^{jJ} = \begin{bmatrix} \cos\theta & \sin\theta & 0 \\ -\sin\theta & \cos\theta & 0 \\ 0 & 0 & 1 \end{bmatrix} \begin{pmatrix} \cos\chi\cos\omega_\oplus T & \cos\chi\sin\omega_\oplus T & -\sin\chi \\ -\sin\omega_\oplus T & \cos\omega_\oplus T & 0 \\ \sin\chi\cos\omega_\oplus T & \sin\chi\sin\omega_\oplus T & \cos\chi \end{pmatrix}, \tag{5}$$

here, T is the sidereal time, χ the colatitude of the lab, and $\omega_\oplus \simeq 2\pi/(23\text{h}56\,\text{min})$ the Earth's sidereal frequency. Therefore, the T-dependence violating coefficients $(\bar{k}_{eff})_{jklm}$ (in the lab frame) can be connected to the constant violating coefficients (in the SME frame) with the following transformation,

$$(\bar{k}_{eff})_{jklm} = R^{jJ}R^{kK}R^{lL}R^{mM}(\bar{k}_{eff})_{JKLM}, \tag{6}$$

take the Equations (4)–(6) into Equation (3), the Lorentz violation potential between two masses can be correspondingly written as a Fourier series

$$V_{\text{LV}}(\theta, \vec{r}, T) = \frac{-Gm_1m_2}{r^3}[c_0 + \sum_{m=1}^{4}(c_m\cos m\omega_\oplus T + s_m\sin m\omega_\oplus T)]. \tag{7}$$

According to Equation (6), the Fourier amplitudes c_0, c_m, and s_m in Equation (7) are functions of $(\bar{k}_{eff})_{JKLM}$. As double trace $(\bar{k}_{eff})_{JKJK}$ is a rotational scalar, it can not be observed in gravitational experiments. Therefore, one can set the double trace $(\bar{k}_{eff})_{JKJK} = 0$, and only fourteen coefficients can be measured in experiments. To simplify the analysis, $(\bar{k}_{eff})_{JKLM}$ can be replaced by the modified coefficients $\bar{k}_j$ (j = 1,2,3, $\cdots$ 14) with a transformation,

$$\begin{bmatrix} \bar{k}_1 \\ \bar{k}_2 \\ \bar{k}_3 \\ \bar{k}_4 \\ \bar{k}_5 \\ \bar{k}_6 \\ \bar{k}_7 \\ \bar{k}_8 \\ \bar{k}_9 \\ \bar{k}_{10} \\ \bar{k}_{11} \\ \bar{k}_{12} \\ \bar{k}_{13} \\ \bar{k}_{14} \end{bmatrix} = \begin{bmatrix} 1 & 1 & 2 & 0 & 0 & 0 & 0 & 0 & 0 & 0 & 0 & 0 & 0 & 0 \\ 0 & 0 & 0 & 1 & 1 & 0 & 0 & 0 & 0 & 0 & 0 & 0 & 0 & 0 \\ 1 & -1 & 0 & 0 & 0 & 0 & 0 & 0 & 0 & 0 & 0 & 0 & 0 & 0 \\ 0 & 0 & 0 & 1 & -1 & 0 & 0 & 0 & 0 & 0 & 0 & 0 & 0 & 0 \\ 0 & 0 & 0 & 0 & 0 & 1 & 1 & 0 & 0 & 0 & 0 & 0 & 0 & 0 \\ 0 & 0 & 0 & 0 & 0 & 0 & 0 & 1 & 0 & 0 & 0 & 0 & 0 & 0 \\ -1 & -1 & 6 & 0 & 0 & 0 & 0 & 0 & 0 & 0 & 0 & 0 & 0 & 0 \\ 0 & 0 & 0 & 0 & 0 & 1 & -1 & 0 & 0 & 0 & 0 & 0 & 0 & 0 \\ 0 & 0 & 0 & 0 & 0 & 0 & 0 & 0 & 1 & 0 & 0 & 0 & 0 & 0 \\ 0 & 0 & 0 & 0 & 0 & 0 & 0 & 0 & 0 & 1 & 0 & 0 & 0 & 0 \\ 0 & 0 & 0 & 0 & 0 & 0 & 0 & 0 & 0 & 0 & 1 & 0 & 0 & 1 \\ 0 & 0 & 0 & 0 & 0 & 0 & 0 & 0 & 0 & 0 & 0 & 1 & 1 & 0 \\ 0 & 0 & 0 & 0 & 0 & 0 & 0 & 0 & 0 & 0 & 1 & 0 & 0 & -3 \\ 0 & 0 & 0 & 0 & 0 & 0 & 0 & 0 & 0 & 0 & 0 & 1 & -3 & 0 \end{bmatrix} \begin{bmatrix} (\bar{k}_{eff})_{XXXX} \\ (\bar{k}_{eff})_{YYYY} \\ (\bar{k}_{eff})_{XXYY} \\ (\bar{k}_{eff})_{XXZZ} \\ (\bar{k}_{eff})_{YYZZ} \\ (\bar{k}_{eff})_{XXXY} \\ (\bar{k}_{eff})_{XYYY} \\ (\bar{k}_{eff})_{XYZZ} \\ (\bar{k}_{eff})_{XZZZ} \\ (\bar{k}_{eff})_{YZZZ} \\ (\bar{k}_{eff})_{XXXZ} \\ (\bar{k}_{eff})_{YYYZ} \\ (\bar{k}_{eff})_{XXYZ} \\ (\bar{k}_{eff})_{XYYZ} \end{bmatrix}. \tag{8}$$

Here, the transforming matrix is obtained by decomposing the corrected factor $k(\hat{r}, T)$, expressed in the Fourier series of Equation (7), into even and odd harmonics and further decomposing the even

part into three terms with the frequencies at 0, $2\omega_\oplus$ and $4\omega_\oplus$ and the odd part into two terms with the frequencies at $\omega_\oplus$ and $3\omega_\oplus$. The detailed description can also be found in the reference [24]. Then the relationship between the predigested coefficients $\bar{k}_j$ and nine Fourier amplitudes can be expressed as,

$$\begin{aligned}
c_0 &= \lambda_1\bar{k}_1 + \lambda_2\bar{k}_2 \\
c_2 &= \lambda_3\bar{k}_3 + \lambda_4\bar{k}_4 + \lambda_5\bar{k}_5 + \lambda_6\bar{k}_6 \\
s_2 &= -\tfrac{1}{2}\lambda_5\bar{k}_3 - \tfrac{1}{2}\lambda_6\bar{k}_4 + 2\lambda_3\bar{k}_5 + 2\lambda_4\bar{k}_6 \\
c_4 &= \lambda_7\bar{k}_7 + \lambda_8\bar{k}_8 \\
s_4 &= \tfrac{1}{4}\lambda_8\bar{k}_7 - 4\lambda_7\bar{k}_8 \\
c_1 &= \lambda_9\bar{k}_9 + \lambda_{10}\bar{k}_{10} + \lambda_{11}\bar{k}_{11} + \lambda_{12}\bar{k}_{12} \\
s_1 &= -\lambda_{10}\bar{k}_9 + \lambda_9\bar{k}_{10} - \lambda_{12}\bar{k}_{11} + \lambda_{11}\bar{k}_{12} \\
c_3 &= \lambda_{13}\bar{k}_{13} + \lambda_{14}\bar{k}_{14} \\
s_3 &= \lambda_{14}\bar{k}_{13} - \lambda_{13}\bar{k}_{14}
\end{aligned} \quad . \tag{9}$$

By introducing the rotation

$$\begin{cases}
\tilde{x} = x\cos\theta\cos\chi - y\sin\theta\cos\chi + z\sin\chi \\
\tilde{y} = x\sin\theta + y\cos\theta \\
\tilde{z} = -x\cos\theta\sin\chi + y\sin\theta\sin\chi + z\cos\chi
\end{cases}, \tag{10}$$

$\lambda_j(\theta,\hat{r},\chi)$ can be further written as

$$\begin{cases}
\lambda_1(\theta,\hat{r},\chi) = -\dfrac{27}{16} + \dfrac{63}{8r^2}\tilde{z}^2 - \dfrac{75}{16r^4}\tilde{z}^4 & \lambda_2(\theta,\hat{r},\chi) = -\dfrac{9}{2} + \dfrac{36}{r^2}\tilde{z}^2 - \dfrac{75}{2r^4}\tilde{z}^4 \\
\lambda_3(\theta,\hat{r},\chi) = -\dfrac{9}{2}\dfrac{\tilde{x}^2-\tilde{y}^2}{r^2} + \dfrac{15}{4}\dfrac{\tilde{x}^4-\tilde{y}^4}{r^4} & \lambda_4(\theta,\hat{r},\chi) = -\dfrac{9}{2}\dfrac{\tilde{x}^2-\tilde{y}^2}{r^2}\left(1-5\dfrac{\tilde{z}^2}{r^2}\right) \\
\lambda_5(\theta,\hat{r},\chi) = \dfrac{\tilde{x}\tilde{y}}{r^2}\left(-18+15\dfrac{\tilde{x}^2+\tilde{y}^2}{r^2}\right) & \lambda_6(\theta,\hat{r},\chi) = 18\dfrac{\tilde{x}\tilde{y}}{r^2}\left(-1+5\dfrac{\tilde{z}^2}{r^2}\right) \\
\lambda_7(\theta,\hat{r},\chi) = \dfrac{45}{8}\dfrac{\tilde{x}^2\tilde{y}^2}{r^4} - \dfrac{15}{16}\dfrac{\tilde{x}^4+\tilde{y}^4}{r^4} & \lambda_8(\theta,\hat{r},\chi) = 15\dfrac{\tilde{x}\tilde{y}}{r^2}\dfrac{\tilde{x}^2-\tilde{y}^2}{r^2} \\
\lambda_9(\theta,\hat{r},\chi) = \dfrac{-\tilde{x}\tilde{z}}{r^2}(18-30\dfrac{\tilde{z}^2}{r^2}) & \lambda_{10}(\theta,\hat{r},\chi) = \dfrac{\tilde{z}\tilde{y}}{r^2}\left(-18+30\dfrac{\tilde{z}^2}{r^2}\right) \\
\lambda_{11}(\theta,\hat{r},\chi) = \dfrac{-\tilde{x}\tilde{z}}{r^2}\left(18-\dfrac{45}{2}\dfrac{\tilde{x}^2+\tilde{y}^2}{r^2}\right) & \lambda_{12}(\theta,\hat{r},\chi) = \dfrac{-\tilde{z}\tilde{y}}{r^2}\left(18-\dfrac{45}{2}\dfrac{\tilde{x}^2+\tilde{y}^2}{r^2}\right) \\
\lambda_{13}(\theta,\hat{r},\chi) = \dfrac{15}{2}\dfrac{-\tilde{x}\tilde{z}}{r^2}\dfrac{3\tilde{y}^2-\tilde{x}^2}{r^2} & \lambda_{14}(\theta,\hat{r},\chi) = \dfrac{45}{2}\dfrac{-\tilde{z}\tilde{y}}{r^2}\dfrac{\tilde{x}^2-\tilde{y}^2/3}{r^2}
\end{cases}, \tag{11}$$

and the relation between Fourier amplitudes and LLI violation coefficients can be shown as,

$$\begin{bmatrix} c_0 \\ c_2 \\ s_2 \\ c_4 \\ s_4 \\ c_1 \\ s_1 \\ c_3 \\ s_3 \end{bmatrix} = \begin{bmatrix} \lambda_1 & 2\lambda_1 & \lambda_1 & \lambda_2 & \lambda_2 & 0 & 0 & 0 & 0 & 0 & 0 & 0 & 0 & 0 \\ \lambda_3 & -\lambda_3 & 0 & \lambda_4 & -\lambda_4 & \lambda_5 & \lambda_5 & \lambda_6 & 0 & 0 & 0 & 0 & 0 & 0 \\ \frac{-\lambda_5}{2} & \frac{\lambda_5}{2} & 0 & \frac{-\lambda_6}{2} & \frac{\lambda_6}{2} & 2\lambda_3 & 2\lambda_3 & 2\lambda_4 & 0 & 0 & 0 & 0 & 0 & 0 \\ -\lambda_7 & -\lambda_7 & 6\lambda_7 & 0 & 0 & \lambda_8 & -\lambda_8 & 0 & 0 & 0 & 0 & 0 & 0 & 0 \\ \frac{-\lambda_8}{4} & \frac{-\lambda_8}{4} & \frac{3\lambda_8}{2} & 0 & 0 & -4\lambda_7 & 4\lambda_7 & 0 & 0 & 0 & 0 & 0 & 0 & 0 \\ 0 & 0 & 0 & 0 & 0 & 0 & 0 & 0 & \lambda_9 & \lambda_{10} & \lambda_{11} & \lambda_{12} & \lambda_{12} & \lambda_{11} \\ 0 & 0 & 0 & 0 & 0 & 0 & 0 & 0 & -\lambda_{10} & \lambda_9 & \lambda_{11} & \lambda_{11} & \lambda_{11} & -\lambda_{12} \\ 0 & 0 & 0 & 0 & 0 & 0 & 0 & 0 & 0 & 0 & \lambda_{13} & \lambda_{14} & -3\lambda_{14} & -3\lambda_{13} \\ 0 & 0 & 0 & 0 & 0 & 0 & 0 & 0 & 0 & 0 & \lambda_{14} & -\lambda_{13} & 3\lambda_{13} & -3\lambda_{14} \end{bmatrix} \begin{bmatrix} (\bar{k}_{eff})_{XXXX} \\ (\bar{k}_{eff})_{YYYY} \\ (\bar{k}_{eff})_{XXYY} \\ (\bar{k}_{eff})_{XXZZ} \\ (\bar{k}_{eff})_{YYZZ} \\ (\bar{k}_{eff})_{XXXY} \\ (\bar{k}_{eff})_{XYYY} \\ (\bar{k}_{eff})_{XYZZ} \\ (\bar{k}_{eff})_{XZZZ} \\ (\bar{k}_{eff})_{YZZZ} \\ (\bar{k}_{eff})_{XXXZ} \\ (\bar{k}_{eff})_{YYYZ} \\ (\bar{k}_{eff})_{XXYZ} \\ (\bar{k}_{eff})_{XYYZ} \end{bmatrix}. \quad (12)$$

Based on this equation, we can search for the LLI violation effect through the experimental data.

2.2. LLI Violation: Spherical Coefficients

Based on the lab frame, LLI violation coefficients can also be expressed by spherical decomposition. Spherical coefficients provide a clean separation of the observable harmonics in sidereal time and offer a direct path for analyses seeking effects of Lorentz violation at arbitrary d. Therefore, the Lorentz violation potential for $d = 6$, in terms of the spherical coordinates r, θ, and ϕ in the lab frame, can be written as,

$$V_{\mathrm{LV}}(\vec{r}) = -G \sum_{jm} \frac{m_1 m_2}{r^3} Y_{jm}(\theta, \phi) k^{\mathrm{lab}}_{jm}, \quad (13)$$

where k^{lab}_{jm} are the spherical coefficients representing the LLI violating effect in the lab frame, which can be related to the SME frame coefficients through the relation [37],

$$k^{\mathrm{lab}}_{jm} = \sum_{m'} e^{im\theta} e^{im'\omega_\oplus T} d^{(j)}_{mm'}(-\chi) k_{jm'}. \quad (14)$$

Here, j in the k^{lab}_{jm} equals to 2 or 4 for $d = 6$, m varies from $-j, \cdots j$, when m is positive or negative, k_{jm} is correspondingly $\mathrm{Re}k_{j,m}$ or $\mathrm{Im}k_{j,m}$, and $d^{(j)}_{mm'}$ is the little Wigner matrices representing the rotation with respect to the y axis. The LLI violation potential in the lab experiments can be regarded as oscillatory with period T and frequency $\omega_\oplus$. Therefore, the LLI violating force varies with the frequencies including the fourth harmonic of $\omega_\oplus$, and it is also the functions of fourteen independently non-relativistic coefficients k_{jm}. Here, to compare them easily, we assume that the relation with respect to spherical coefficients between Fourier amplitudes and transfer coefficients has the similar transforming form to cartesian coefficients. Then, the nine Fourier amplitudes in Equation (7) can be expressed by the spherical coefficients as

$$
\begin{aligned}
c_0 &= \gamma_1 k_{2,0} + \gamma_2 k_{4,0} \\
c_2 &= \gamma_3 \mathrm{Re}k_{2,2} + \gamma_4 \mathrm{Im}k_{2,2} + \gamma_5 \mathrm{Re}k_{4,2} + \gamma_6 \mathrm{Im}k_{4,2} \\
s_2 &= \gamma_4 \mathrm{Re}k_{2,2} - \gamma_3 \mathrm{Im}k_{2,2} + \gamma_6 \mathrm{Re}k_{4,2} - \gamma_5 \mathrm{Im}k_{4,2} \\
c_4 &= \gamma_7 \mathrm{Re}k_{4,4} + \gamma_8 \mathrm{Im}k_{4,4} \\
s_4 &= \gamma_8 \mathrm{Re}k_{4,4} - \gamma_7 \mathrm{Im}k_{4,4} \\
c_3 &= \gamma_{13} \mathrm{Re}k_{4,3} + \gamma_{14} \mathrm{Im}k_{4,3} \\
s_3 &= \gamma_{14} \mathrm{Re}k_{4,3} - \gamma_{13} \mathrm{Im}k_{4,3}
\end{aligned}
\quad , \tag{15}
$$

which have been written with cartesian coefficients, shown in Equation (9). The final expression for violation coefficients (cartesian coefficients or spherical coefficients) can be transformed to each other by a transformation matrix [37], and the relation of k_{jm} and $(\bar{k}_{eff})_{JKLM}$ can be shown as

$$
\begin{bmatrix}
k_{2,0} \\ \mathrm{Re}k_{2,1} \\ k_{2,-1} \\ \mathrm{Re}k_{2,2} \\ \mathrm{Im}k_{2,-2} \\ k_{4,0} \\ \mathrm{Re}k_{4,1} \\ \mathrm{Im}k_{4,-1} \\ \mathrm{Re}k_{4,2} \\ \mathrm{Im}k_{4,-2} \\ \mathrm{Re}k_{4,3} \\ \mathrm{Im}k_{4,-3} \\ \mathrm{Re}k_{4,4} \\ \mathrm{Im}k_{4,-4}
\end{bmatrix}
= \frac{\sqrt{\pi}}{7}
\begin{bmatrix}
\frac{36}{\sqrt{5}} & 0 & 0 & \frac{72}{\sqrt{5}} & 0 & \frac{36}{\sqrt{5}} & 0 & 0 & 0 & 0 & \frac{36}{\sqrt{5}} & 0 & \frac{36}{\sqrt{5}} & 0 \\
0 & 0 & \frac{12\sqrt{6}}{\sqrt{5}} & 0 & 0 & 0 & 0 & \frac{12\sqrt{6}}{\sqrt{5}} & 0 & \frac{12\sqrt{6}}{\sqrt{5}} & 0 & 0 & 0 & 0 \\
0 & 0 & 0 & 0 & \frac{-12\sqrt{6}}{\sqrt{5}} & 0 & 0 & 0 & 0 & 0 & 0 & \frac{-12\sqrt{6}}{\sqrt{5}} & 0 & \frac{-12\sqrt{6}}{\sqrt{5}} \\
\frac{-6\sqrt{6}}{\sqrt{5}} & 0 & 0 & 0 & 0 & \frac{-6\sqrt{6}}{\sqrt{5}} & 0 & 0 & 0 & 0 & \frac{6\sqrt{6}}{\sqrt{5}} & 0 & \frac{6\sqrt{6}}{\sqrt{5}} & 0 \\
0 & \frac{12\sqrt{6}}{\sqrt{5}} & 0 & 0 & 0 & 0 & \frac{12\sqrt{6}}{\sqrt{5}} & 0 & \frac{12\sqrt{6}}{\sqrt{5}} & 0 & 0 & 0 & 0 & 0 \\
-5 & 0 & 0 & -10 & 0 & \frac{-40\sqrt{10}}{7} & 0 & 0 & 0 & 0 & -5 & 0 & -40 & 0 \\
0 & 0 & 6 & 0 & 0 & 0 & 0 & 6 & 0 & -8 & 0 & 0 & 0 & 0 \\
0 & 0 & 0 & 0 & -6 & 0 & 0 & 0 & 0 & 0 & 0 & -6 & 0 & 8 \\
-\sqrt{10} & 0 & 0 & 0 & 0 & -10\sqrt{5} & 0 & 0 & 0 & 0 & \sqrt{10} & 0 & -6\sqrt{10} & 0 \\
0 & 2\sqrt{10} & 0 & 0 & 0 & 0 & 2\sqrt{10} & 0 & -12\sqrt{10} & 0 & 0 & 0 & 0 & 0 \\
0 & 0 & -2\sqrt{35} & 0 & 0 & 0 & 0 & 6\sqrt{35} & 0 & 0 & 0 & 0 & 0 & 0 \\
0 & 0 & 0 & 0 & 6\sqrt{35} & 0 & 0 & 0 & 0 & 0 & 0 & -2\sqrt{35} & 0 & 0 \\
\frac{\sqrt{5}}{\sqrt{2}} & 0 & 0 & -3\sqrt{70} & 0 & 0 & 0 & 0 & 0 & 0 & \frac{\sqrt{5}}{\sqrt{2}} & 0 & 0 & 0 \\
0 & -2\sqrt{70} & 0 & 0 & 0 & 0 & 2\sqrt{70} & 0 & 0 & 0 & 0 & 0 & 0 & 0
\end{bmatrix}
\begin{bmatrix}
(\bar{k}_{eff})_{XXXX} \\ (\bar{k}_{eff})_{XXXY} \\ (\bar{k}_{eff})_{XXXZ} \\ (\bar{k}_{eff})_{XXYY} \\ (\bar{k}_{eff})_{XXYZ} \\ (\bar{k}_{eff})_{XXZZ} \\ (\bar{k}_{eff})_{XYYY} \\ (\bar{k}_{eff})_{XYYZ} \\ (\bar{k}_{eff})_{XYZZ} \\ (\bar{k}_{eff})_{XZZZ} \\ (\bar{k}_{eff})_{YYYY} \\ (\bar{k}_{eff})_{YYYZ} \\ (\bar{k}_{eff})_{YYZZ} \\ (\bar{k}_{eff})_{YZZZ}
\end{bmatrix} . \tag{16}
$$

Combining this transformation and Equation (11), γ_j can be obtained as

$$
\begin{cases}
\gamma_1 = -\frac{\sqrt{5}}{4\sqrt{\pi}}(1 - 3\frac{\tilde{z}^2}{r^2}) & \gamma_2 = \frac{1}{16\sqrt{\pi}}(9 - 90\frac{\tilde{z}^2}{r^2} - 105\frac{\tilde{z}^4}{r^4}) \\
\gamma_3 = -\frac{\sqrt{15}}{2\sqrt{2\pi}}(\frac{\tilde{x}^2 - \tilde{y}^2}{r^2}) & \gamma_4 = -\frac{\sqrt{15}}{2\sqrt{2\pi}}\frac{\tilde{x}\tilde{y}}{r^2} \\
\gamma_5 = \frac{3\sqrt{5}}{4\sqrt{2\pi}}\frac{\tilde{x}^2 - \tilde{y}^2}{r^2}(1 - 7\frac{\tilde{z}^2}{r^2}) & \gamma_6 = \frac{3\sqrt{5}}{2\sqrt{2\pi}}\frac{\tilde{x}\tilde{y}}{r^2}(1 - 7\frac{\tilde{z}^2}{r^2}) \\
\gamma_7 = \frac{3\sqrt{35}}{8\sqrt{2\pi}}\frac{\tilde{x}^4 - 6\tilde{x}^2\tilde{y}^2 + \tilde{y}^4}{r^4} & \gamma_8 = \frac{3\sqrt{35}}{\sqrt{2\pi}}\frac{\tilde{x}\tilde{y}}{r^2}\frac{\tilde{x}^2 - \tilde{y}^2}{r^2} \\
\gamma_9 = \frac{\sqrt{15}}{\sqrt{2\pi}}\frac{\tilde{x}\tilde{y}}{r^2} & \gamma_{10} = -\frac{\sqrt{15}}{\sqrt{2\pi}}\frac{\tilde{y}\tilde{z}}{r^2} \\
\gamma_{11} = -\frac{3\sqrt{5}}{4\sqrt{\pi}}\frac{\tilde{x}\tilde{z}}{r^2}(3 - 7\frac{\tilde{z}^2}{r^2}) & \gamma_{12} = \frac{3\sqrt{5}}{4\sqrt{\pi}}\frac{\tilde{y}\tilde{z}}{r^2}(3 - 7\frac{\tilde{z}^2}{r^2}) \\
\gamma_{13} = \frac{3\sqrt{35}}{4\sqrt{\pi}}\frac{\tilde{x}\tilde{z}}{r^2}\frac{\tilde{x}^2 - 3\tilde{y}^2}{r^2} & \gamma_{14} = -\frac{3\sqrt{35}}{4\sqrt{\pi}}\frac{\tilde{y}\tilde{z}}{r^2}\frac{\tilde{y}^2 - 3\tilde{x}^2}{r^2}
\end{cases} . \tag{17}
$$

As a result, the nine Fourier amplitudes c_0, c_m and s_m are linear combinations of k_{jm}, through the fourteen independent functions $\gamma_j(\theta, \hat{r}, \chi)$ with $j = 1, 2, \cdots 14$.

3. LLI Violation in Pendulum Experiments

In general short-range pendulum experiments, the planar geometry is often used to suppress the Newtonian background, and it also suppresses the LLI violation signal. After the numerical calculation, the Newtonian force between two infinite planes of uniform mass density is constant, and the Lorentz violating force between two infinite planes is zero. In fact, the infinite plate is not existent in true life, so the Lorentz violating force between two planes is not zero, and we find it is dominated by the edge

effect. Based on the experimental data of testing the gravitational inverse square law (HUST-2011) with a pendulum, we have analyzed the LLI violation effect and constrained the violating coefficients at the level of 10^{-8} m^2 [38]. Moreover, we perform a combined analysis and achieved the best level of LLI violation at 10^{-9} m^2 [25]. For our experiments (HUST-2011, HUST-2015), the range and density modulation are adopted to change the interaction between the test and source masses, and we measure the variation of torque to extract the LLI violating signal, while IU experiments (IU-2002 and IU-2012) measure the force variation at a shorter range.

We now analyze the LLI violating signal between the test (density ρ_1) and source (density ρ_2) masses in a pendulum experiment. With the assumption of $dm_1 = \rho_1 dV_1$ and $dm_2 = \rho_2 dV_2$, the Lorentz violation torque can be expressed by cartesian coefficients and spherical coefficients as

$$\begin{aligned}\tau_{LV} &= G\rho_1\rho_2 \iint dV_1 dV_2 \frac{\partial}{\partial\theta_1}\frac{k(\vec{r})}{r^3} = G\rho_1\rho_2 \iint dV_1 dV_2 \frac{\partial}{\partial\theta_1}\frac{\sum\limits_{jm} Y_{jm}(\theta,\phi)k^{lab}_{jm}}{r^3} \\ &= G\rho_1\rho_2 \iint dV_1 dV_2 \frac{\partial}{\partial\theta_1}\frac{c_0 + \sum\limits_{m=1}^{4} c_m \cos(m\omega_\oplus T) + s_m sin(m\omega_\oplus T)}{r^3}\end{aligned} \quad , \quad . \tag{18}$$

with θ_1 the angle between torque balance and source mass in horizontal direction. Comparing with Equation (9), the transfer coefficients with cartesian coefficients and spherical coefficients can be shown as,

$$\begin{aligned}\Lambda_j &= G\rho_1\rho_2 \iint \frac{\partial}{\partial\theta_1}\frac{\lambda_j(\theta,\hat{r},\chi)}{r^3} dV_1 dV_2 \\ \Gamma_j &= G\rho_1\rho_2 \iint \frac{\partial}{\partial\theta_1}\frac{\gamma_j(\theta,\hat{r},\chi)}{r^3} dV_1 dV_2\end{aligned} \quad . \tag{19}$$

The Lorentz violation torque can be similarly expanded as the Fourier series,

$$\tau_{LV} = C_0 + \sum_{m=1}^{4} [C_m \cos(m\omega_\oplus T) + S_m \sin(m\omega_\oplus T)], \tag{20}$$

then the specific relation between the Fourier amplitudes and the LLI violation coefficients can be written as

$$\begin{bmatrix} C_0 \\ C_2 \\ S_2 \\ C_4 \\ S_4 \\ C_1 \\ S_1 \\ C_3 \\ S_3 \end{bmatrix} = \begin{bmatrix} \Lambda_1 & 2\Lambda_1 & \Lambda_1 & \Lambda_2 & \Lambda_2 & 0 & 0 & 0 & 0 & 0 & 0 & 0 & 0 & 0 \\ \Lambda_3 & -\Lambda_3 & 0 & \Lambda_4 & -\Lambda_4 & \Lambda_5 & \Lambda_5 & \Lambda_6 & 0 & 0 & 0 & 0 & 0 & 0 \\ \frac{-\Lambda_5}{2} & \frac{\Lambda_5}{2} & 0 & \frac{-\Lambda_6}{2} & \frac{\Lambda_6}{2} & 2\Lambda_3 & 2\Lambda_3 & 2\Lambda_4 & 0 & 0 & 0 & 0 & 0 & 0 \\ -\Lambda_7 & -\Lambda_7 & 6\Lambda_7 & 0 & 0 & \Lambda_8 & -\lambda_8 & 0 & 0 & 0 & 0 & 0 & 0 & 0 \\ \frac{-\Lambda_8}{4} & \frac{-\Lambda_8}{4} & \frac{3\Lambda_8}{2} & 0 & 0 & -4\Lambda_7 & 4\Lambda_7 & 0 & 0 & 0 & 0 & 0 & 0 & 0 \\ 0 & 0 & 0 & 0 & 0 & 0 & 0 & 0 & \Lambda_9 & \Lambda_{10} & \Lambda_{11} & \Lambda_{12} & \Lambda_{12} & \Lambda_{11} \\ 0 & 0 & 0 & 0 & 0 & 0 & 0 & 0 & -\Lambda_{10} & \Lambda_9 & \Lambda_{11} & \Lambda_{11} & \Lambda_{11} & -\Lambda_{12} \\ 0 & 0 & 0 & 0 & 0 & 0 & 0 & 0 & 0 & 0 & \Lambda_{13} & \Lambda_{14} & -3\Lambda_{14} & -3\Lambda_{13} \\ 0 & 0 & 0 & 0 & 0 & 0 & 0 & 0 & 0 & 0 & \Lambda_{14} & -\Lambda_{13} & 3\Lambda_{13} & -3\Lambda_{14} \end{bmatrix} \begin{bmatrix} (\bar{k}_{eff})_{XXXX} \\ (\bar{k}_{eff})_{YYYY} \\ (\bar{k}_{eff})_{XXYY} \\ (\bar{k}_{eff})_{XXZZ} \\ (\bar{k}_{eff})_{YYZZ} \\ (\bar{k}_{eff})_{XXXY} \\ (\bar{k}_{eff})_{XYYY} \\ (\bar{k}_{eff})_{XYZZ} \\ (\bar{k}_{eff})_{XZZZ} \\ (\bar{k}_{eff})_{YZZZ} \\ (\bar{k}_{eff})_{XXXZ} \\ (\bar{k}_{eff})_{YYYZ} \\ (\bar{k}_{eff})_{XXYZ} \\ (\bar{k}_{eff})_{XYYZ} \end{bmatrix} \tag{21}$$

in cartesian coefficients, and

$$\begin{bmatrix} C_0 \\ C_2 \\ S_2 \\ C_4 \\ S_4 \\ C_1 \\ S_1 \\ C_3 \\ S_3 \end{bmatrix} = \begin{bmatrix} \Gamma_1 & \Gamma_2 & 0 & 0 & 0 & 0 & 0 & 0 & 0 & 0 & 0 & 0 & 0 & 0 \\ 0 & 0 & \Gamma_3 & \Gamma_4 & \Gamma_5 & \Gamma_6 & 0 & 0 & 0 & 0 & 0 & 0 & 0 & 0 \\ 0 & 0 & \Gamma_4 & -\Gamma_3 & \Gamma_6 & -\Gamma_5 & 0 & 0 & 0 & 0 & 0 & 0 & 0 & 0 \\ 0 & 0 & 0 & 0 & 0 & 0 & \Gamma_7 & \Gamma_8 & 0 & 0 & 0 & 0 & 0 & 0 \\ 0 & 0 & 0 & 0 & 0 & 0 & \Gamma_8 & -\Gamma_7 & 0 & 0 & 0 & 0 & 0 & 0 \\ 0 & 0 & 0 & 0 & 0 & 0 & 0 & 0 & \Gamma_9 & \Gamma_{10} & \Gamma_{11} & \Gamma_{12} & 0 & 0 \\ 0 & 0 & 0 & 0 & 0 & 0 & 0 & 0 & \Gamma_{10} & -\Gamma_9 & \Gamma_{12} & -\Gamma_{11} & 0 & 0 \\ 0 & 0 & 0 & 0 & 0 & 0 & 0 & 0 & 0 & 0 & 0 & 0 & \Gamma_{13} & \Gamma_{14} \\ 0 & 0 & 0 & 0 & 0 & 0 & 0 & 0 & 0 & 0 & 0 & 0 & \Gamma_{14} & -\Gamma_{13} \end{bmatrix} \begin{bmatrix} k_{2,0} \\ k_{4,0} \\ \mathrm{Re}\, k_{2,2} \\ \mathrm{Im}\, k_{2,2} \\ \mathrm{Re}\, k_{4,2} \\ \mathrm{Im}\, k_{4,2} \\ \mathrm{Re}\, k_{4,4} \\ \mathrm{Im}\, k_{4,4} \\ \mathrm{Re}\, k_{2,1} \\ \mathrm{Im}\, k_{2,1} \\ \mathrm{Re}\, k_{4,1} \\ \mathrm{Im}\, k_{4,1} \\ \mathrm{Re}\, k_{4,3} \\ \mathrm{Im}\, k_{4,3} \end{bmatrix} \quad (22)$$

in spherical coefficients. Based on Equations (21) and (22), C_0 is a linear combination of Λ_1 and Λ_2 or Γ_1 and Γ_2. C_2, S_2 are the linear combinations of Λ_3, Λ_4, Λ_5 and Λ_6 or Γ_3, Γ_4, Γ_5 and Γ_6. C_4, S_4 are the linear combinations of Λ_7 and Λ_8 or Γ_7 and Γ_8. C_1, S_2 are the linear combinations of Λ_9, Λ_{10}, Λ_{11} and Λ_{12} or Γ_9, Γ_{10} ,Γ_{11} and Γ_{12}. C_3, S_3 are the linear combinations of Λ_{13} and Λ_{14} or Γ_{13} and Γ_{14}. As a result, we can achieve the spherical coefficients k_{jm} and descartes coefficients $(\bar{k}_{eff})_{JKLM}$, as long as the Lorentz violation torque is measured. According to Equations (21) and (22), the transfer coefficients can be regarded as the bridge of the LLI violation torque and LLI violation coefficients. Based on Equation (16), the relation of transfer coefficients with spherical coefficients and cartesian coefficients can be expressed as

$$\begin{cases} \Gamma_1 = \frac{5(8\Lambda_1 - 5\Lambda_2)}{36\sqrt{5\pi}} & \Gamma_2 = \frac{\Lambda_1 - \Lambda_2}{5\sqrt{\pi}} \\ \Gamma_3 = \frac{-\sqrt{5/6\pi}}{6}(6\Lambda_3 + \Lambda_4) & \Gamma_4 = \frac{\sqrt{5/6\pi}}{12}(6\Lambda_5 + \Lambda_6) \\ \Gamma_5 = \frac{\sqrt{5/2\pi}}{5}(\Lambda_4 - \Lambda_3) & \Gamma_3 = \frac{\sqrt{5/2\pi}}{10}(\Lambda_5 - \Lambda_6) \\ \Gamma_7 = -\sqrt{\frac{14}{5\pi}}\Lambda_7 & \Gamma_8 = -\sqrt{\frac{7}{10\pi}}\Lambda_8 \\ \Gamma_9 = \frac{1}{4}\sqrt{\frac{5}{6\pi}}(\Lambda_9 + \frac{4}{3}\Lambda_{11}) & \Gamma_{10} = \frac{1}{4}\sqrt{\frac{5}{6\pi}}(\Lambda_{10} + \frac{4}{3}\Lambda_{12}) \\ \Gamma_9 = \frac{1}{10}\sqrt{\frac{5}{\pi}}(\Lambda_{11} - \Lambda_9) & \Gamma_{10} = \frac{1}{10}\sqrt{\frac{5}{\pi}}(\Lambda_{10} - \Lambda_{12}) \\ \Gamma_{13} = -\frac{1}{2}\sqrt{\frac{7}{5\pi}}\Lambda_{13} & \Gamma_{14} = -\frac{1}{2}\sqrt{\frac{7}{5\pi}}\Lambda_{14} \end{cases} . \quad (23)$$

4. Experimental Design and Expected Result for Testing Lorentz Violation

4.1. Experimental Design

As LLI violation effect is dominated by the edge effect, here, we modify the structure of test and source masses from the flat plate design (see HUST-2011) to the striped design. The detailed description for this new design can be seen in [29], in which the transfer coefficients are improved greatly and the upper bound of the LLI violation coefficients may be improved by about one order of magnitude.

To independently limit the fourteen LLI violation coefficients, we advance two stripe-type designs, horizontal stripe type and vertical stripe type, shown in Figure 1. Here, we will take the horizontal stripe-type setup, for example, to simply introduce this new design. With the same dimensions of 19.8 mm × 19.8 mm × 1.3 mm, two tungsten and horizontally stripped masses (one is the test mass W_t and the other is the counterbalance mass) are symmetrically adhered to the two sides of the I-shaped pendulum, symmetrically. The arm length of the test mass is 41.1 mm. The source mass

platform, facing the pendulum, is also designed as an I-shaped structure. A tungsten source mass (W_s) with dimension 19.8 mm × 19.8 mm × 1.3 mm is adhered to one side of the I-shaped structure, opposite to the test mass W_t. The non-Newtonian torque can be measured between test and source masses for separations from 0.4 to 1.0 mm, where the net change of Newtonian torque is counteracted by a tungsten counterweight mass with dimensions of 19.8 mm × 19.8 mm × 1.3 mm, adhered to the other side of the source mass platform, and located the same to W_t in the y axis direction. The right parts in the experimental setups of (a) and (b) are copper cylinders, which are used to calibrate the gravitational signal. To increase the LLI violation signal and decrease the Newton torque signal at the same time, we come up with a new design, shown in Figure 2: with the positions of test masses (W_t) unchanged, one should shift the left source mass up for half of the width of a strip ($+\pi/2$) and left half of the width of a strip, and shift the right W_s down for half of the width of a strip ($-\pi/2$) and right for half of the width of a strip. In this design, the Newtonian torque between left test and source masses is counteracted by the Newtonian torque between right test and source masses strictly. In other words, this specially tripped design can not only suppress the Newtonian gravitational signal strongly but also enlarge the LLI violating signal.

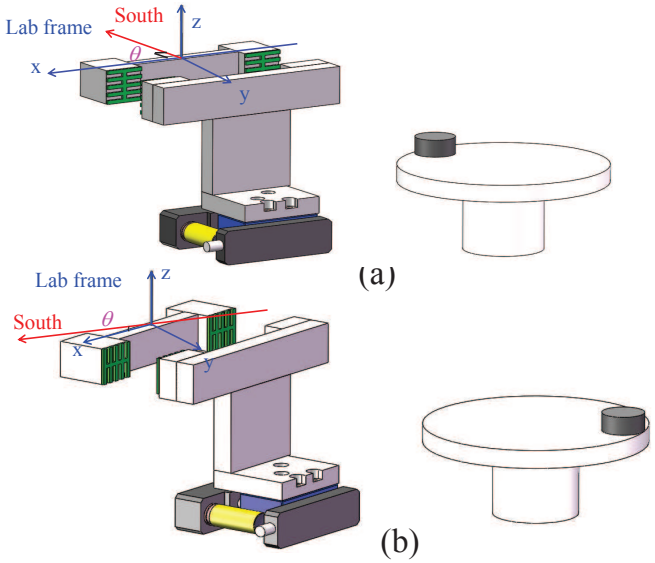

Figure 1. Schematic diagram of the LLI-violation signal-sensitive experimental design. Both the test and source masses are in the periodically stripped geometry (along z direction). (**a**) is horizontal stripe-type geometry with the angle $\theta = \pi/2$ between torsion system and lab system; (**b**) is vertical stripe-type geometry with $\theta = \pi/6$.

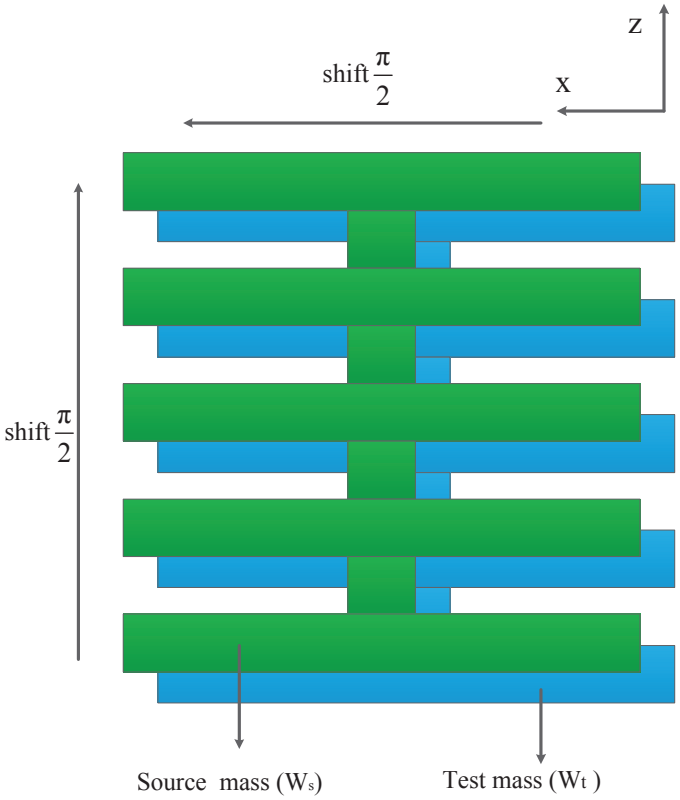

Figure 2. Relative positions between the test (W_t) and source (W_s) masses in the $x-z$ plane. The positions of the test masses (left mass and right mass) are kept invariant in experiments. One source mass is shifted up for half of a strip's width ($+\pi/2$) and left for half of a strip's width.

From Figure 1, to make the transfer coefficients as large as possible, different angles are chosen in (a) and (b). Based on Equation (22), the larger transfer coefficients Γ_j are, the larger LLI violation signal we will achieve, which means the higher limitation of the LLI violation coefficients k_{jm} we will obtain with the same experimental precision. From Equation (19), as θ is involved in the transfer coefficients, we should choose an appropriate angle to make the fourteen transfer coefficients large simultaneously. For the violating signal in the typical short-range pendulum experiments, the uncertainty for the constant mode C_0 is limited by the systematic errors, while the uncertainties for the harmonic modes C_m and S_m are limited by the statistics errors. As the systematic error is lager than the statistics error, the constraints of the violating coefficients related to C_0 are potentially worse than those related to C_m and S_m. Here, to achieve better constraints for the total violating coefficients, we select a better "θ", with which the transferring coefficients for the violating coefficients related to C_0 get the larger values. This can be checked by the numerical simulation. To more directly describe their relation, we list the variation of all transfer coefficients with θ in horizontal stripe-type (see Figure 3) and vertical stripe-type (see Figure 4), respectively. Besides, the appropriate angles in different stripe-type experiments are also denoted in Figures 3 and 4.

For this new experimental design, the LLI violation torque is modulated by changing the separation between the test and source masses. The violating torque can be expanded as a Fourier series, and nine Fourier amplitudes can be extracted from the experiments. Thus, the fourteen Lorentz violation coefficients cannot be obtained by one experiment. Here, we design two stripe-type experiments (see Figure 1a,b) to test the LLI effect. Finally, all fourteen LLI violation coefficients can be extracted from a combined analysis of horizontal and vertical stripe geometry experiments.

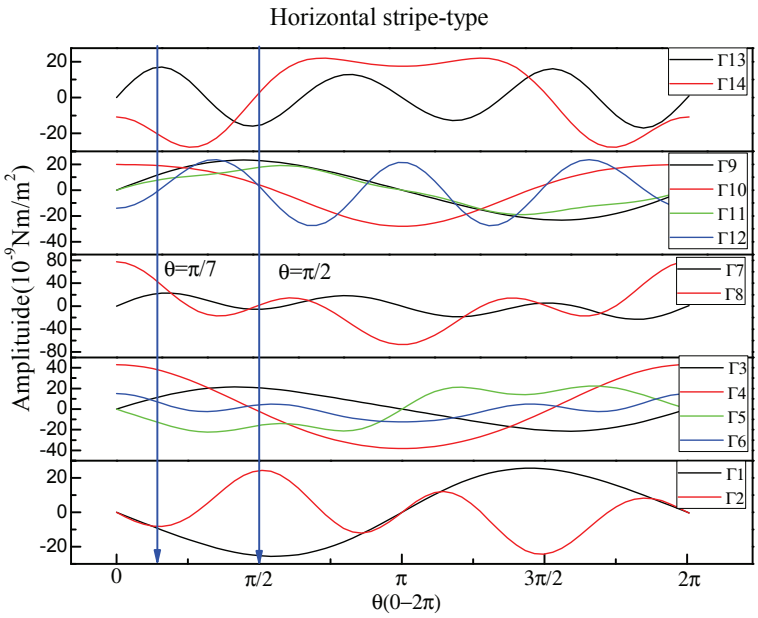

Figure 3. (Color online) The relationship between all fourteen transfer coefficients and angle in horizontal stripe-type experiment. From this figure, the transfer coefficients get larger, when $\theta \approx \pi/7$ or $\pi/2$.

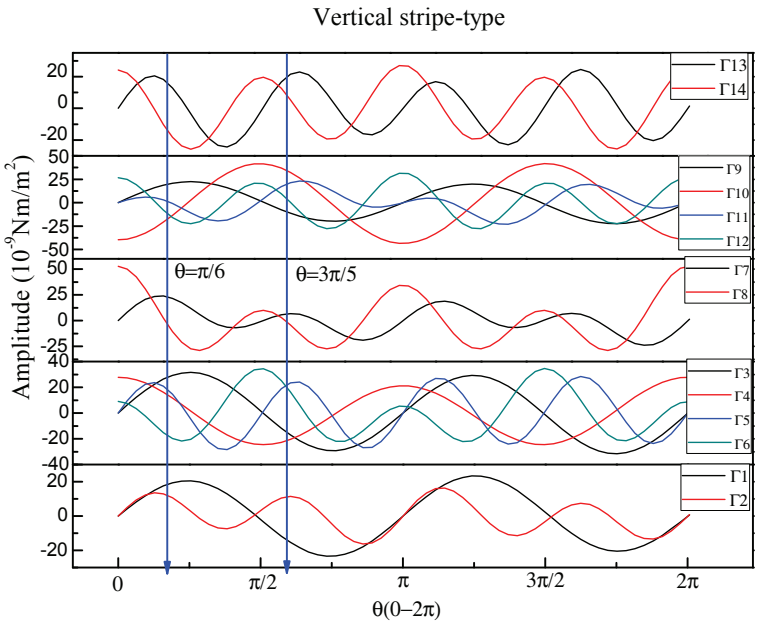

Figure 4. (Color online) The relationship between the fourteen transfer coefficients and angle in vertical stripe-type experiment. From this figure, the transfer coefficients get larger, when $\theta \approx \pi/6$ or $3\pi/5$.

4.2. Discussion and Expected Result

Based on the description of experimental design, at least two experiments are needed to independently give the limit of LLI violation coefficients. In fact, either horizontal stripes experiment or vertical stripes experiment can be operated more than twice with different angles θ. Therefore, to obtain the best constraints for the LLI violation coefficients, the most important thing is to choose a perfect combination.

To choose a suitable combined scheme, we can use the existing experimental error bar to estimate the feasibility of our new stripe-type design. As the new experimental design is based on HUST-2011 experiment, we can estimate the error bar similarly. In HUST-2011 experiment [38], experimental error of the constant term (C_0) and harmonic terms (C_m, S_m) at 2σ have achieved the level at 1.9×10^{-16} Nm and 0.45×10^{-16} Nm, respectively. The error of C_0 is dominant by the systematic error, while the errors of C_m, S_m are limited by the thermal noise, which is at the same level to the statistical errors in current experiment.

The systematic errors related to C_0 are rooted in the machining and aligning of the masses, especially the aligning in experiment. Then, assuming both the machining precision and aligning (no matter along the horizontal direction or the vertical direction) precision are three microns, a whole error estimation for horizontal stripe-type and vertical stripe-type experimental designs can be derived, which are listed in second and third columns of Table 1, respectively. Meanwhile, similar to the HUST-2011 experiment, we also cursorily estimate the thermal noise, which is also listed in Table 1. Moreover, to derive an expected constraints for LLI violation coefficients, we set the errors of C_m, S_m at 0.45×10^{-16} Nm, and C_0 at 11.7×10^{-16} Nm and 10.4×10^{-16} Nm in horizontal and vertical stripe-type structures, respectively.

Based on the above analysis, to independently constrain the LLI violating coefficients with a high limitation, we choose two stripe-type experiments with the same error level for a combining analysis, in which $\theta = \pi/7$ and $\pi/2$ in horizontal stripe-type experiments and $\theta = \pi/6$ and $3\pi/5$ in vertical stripe-type experiments. Finally, we estimate the improvement of the constraints for the LLI violating coefficients, which is shown by the ratio of the total error in the current best constraint to that in our new design, see Table 2. Here, the first column represents the all fourteen spherical coefficients for $d = 6$; the second column gives the current best constraints of LLI violating spherical coefficients; and the last two columns stands for the improvement of the limitation of LLI violation coefficients in horizontal stripe-type and vertical stripe-type designs, respectively.

Table 1. The main errors of constant term amplitude (C_0) in the periodic strip design, which include the metrology errors (assuming the errors on all sources are three microns) and the statistical error (thermal noise).

Sources	Error of C_0 in Horizontal Stripe-Type Design ($\Delta\tau$ (10^{-16}Nm))	Error of C_0 in Vertical Stripe-Type Design ($\Delta\tau$ (10^{-16}Nm))
Size error in test mass	4.0	4.0
Size error in source mass	3.9	3.8
The aligned error in horizontal direction	1.4	5.2
The aligned error in height direction	4.4	0.6
Horizontal error in experimenting	0.8	6.6
Height error in experimenting	9.1	2.5
Statistical error (thermal noise)	0.4	0.4
Total	11.7	10.4

From Table 2, the upper bounds of violation coefficients are all improved in the two stripe-type experiments. However, different coefficients have different improvements. The coefficients related to harmonic frequencies are increased by more than one order of magnitude, while the coefficients related to the constant term just can be increased four or five multiples. Therefore, to effectively improve the constraints of Lorentz violation coefficients, one can ameliorate the precision of experimental material to decrease the system error or extend the length of data to decease the statistical error.

Table 2. The improvement of the constraints for LLI violating spherical coefficients in the new design, which is shown by the ratio of the total error in the current best constraint [37] to that in our new design. (See the last columns of this Table).

Coefficients	Current Constraint (10^{-8} m^2) [37]	Ratio in Horizontal Stripe-Type for $\theta = \pi/7$ and $\pi/2$	Ratio in Vertical Stripe-Type for $\theta = \pi/6$ and $3\pi/5$
$k_{2,0}$	3 ± 23	4	5
Re $k_{1,1}$	-4 ± 4	16	21
Im $k_{2,1}$	-2 ± 4	16	21
Re $k_{2,2}$	0 ± 9	67	73
Im $k_{2,2}$	1 ± 4	30	32
$k_{4,0}$	4 ± 25	4	4
Re $k_{4,1}$	3 ± 5	13	14
Im $k_{4,1}$	1 ± 5	13	14
Re $k_{2,2}$	0 ± 12	44	92
Im $k_{2,2}$	2 ± 2	7	15
Re $k_{4,3}$	0 ± 1	7	7
Im $k_{4,3}$	1 ± 1	7	7
Re $k_{4,4}$	2 ± 9	97	49
Im $k_{4,4}$	2 ± 5	54	27

5. Conclusions

In this paper, we describe an experimental design, increasing the LLI violation signal with the test mass and source mass in the stripe type. With this design, the constraints of all fourteen Lorentz violation coefficients may be improved by about one order of magnitude. In addition, we find that an appropriate value for θ (the angle between the SME and lab frames) can help to give the larger transfer coefficients: for the typical parameters, take $\theta \approx \pi/7$ and $\pi/2$ in the horizontal stripe-type experiments and $\theta \approx \pi/6$ and $3\pi/5$ in the vertical stripe-type experiments, respectively. Finally, we report in Table 2 the expected improvements of the constraints for each LLI violation coefficients with conservative estimation.

Acknowledgments: We gratefully acknowledge support by the National Natural Science Foundation of China (Grants No. 91636221).

Author Contributions: Chenggang Shao conceived this study, led the narrative framing for the paper and coordinated its writing. Yafen Chen provided substantial inputs to writing and significant feedback on numerous drafts. Yujie Tan helped us modify the paper.

Conflicts of Interest: The authors declare no conflict of interest.

References

1. Iorio, L. Editorial for the Special Issue 100 Years of Chronogeometrodynamics: The Status of the Einstein's Theory of Gravitation in Its Centennial Year. *Universe* **2015**, *1*, 1: 38–1:81.
2. Debono, I.; Smoot, G.F. General Relativity and Cosmology: Unsolved Questions and Future Directions. *Universe* **2016**, *2*, 23:1–23:82.
3. Amelino-Camelia, G. Quantum Spacetime Phenomenology. *Living Rev. Relativ.* **2013**, *16*, 5.
4. Kostelecký, V.A.; Samuel, S. Spontaneous Breaking of Lorentz Symmetry in String Theory. *Phys. Rev. D* **1989**, *39*, 683–685.
5. Kostelecký, V.A.; Potting, R. CPT and Strings. *Nucl. Phys.* **1991**, *B359*, 545–570.
6. Kostelecký, V.A.; Potting, R. CPT, Strings, and Meson Factories. *Phys. Rev. D* **1995**, *51*, 3923–3935.
7. Kostelecký, V.A. Gravity, Lorentz Violation, and the Standard Model. *Phys. Rev. D* **2009**, *69*, 105009:1–105009:20.
8. Bailey, Q.G.; Kostelecký, V.A. Signals for Lorentz Violation in Post-Newtonian Gravity. *Phys. Rev. D* **2006**, *74*, 045001.
9. Mattingly, D. Modern Tests of Lorentz Invariance. *Living. Rev. Relativ.* **2005**, *8*, 5:1–5:84.

10. Will, C.M. The confrontation between General Relativity and Experiment. *Living. Rev. Relativ.* **2014**, *17*, 4:1–4:117.
11. Tasson, J.D. The Standard-Model Extension and Gravitational Tests. *Symmetry* **2016**, *8*, 111:1–111:16.
12. Hees, A.; Bailey, Q.G.; Bourgoin, A.; Bars, H.P.; Guerlin, C.; Poncin-Lafitte, C.L. Tests of Lorentz Symmetry in the Gravitational Sector. *Universe* **2016**, *2*, 30:1–30:40.
13. Shao, L.J. Experimental Studies on the Lorentz Symmetry in Post-Newtonian Gravity with Pulsars. *Universe* **2016**, *2*, 29:1–29:5.
14. Iorio, L. Orbital effects of Lorentz-Violating Standard Model Extension Gravitomagnetism around a Static Body: A Sensitivity Analysis. *Class. Quantum Gravity* **2012**, *29*, 175007:1–175007:7.
15. Will, C.M.; Nordtvent, K. Conservation Laws and Preferred Frames in Relativistic Gravity. I: Preferred-Frame Theories and an Extended PPN Formalism. *Astrophys. J.* **1972**, *284*, 27360:1–27360:37.
16. Shao, L.J.; Caballero, R.N.; Kramer, M.; Wex, N.; Champion, D.J.; Jessner, A. A New Limit on Local Lorentz Invariance Violation of Gravity from Solitary Pulsars. *Class. Quantum Gravity* **2013**, *30*, 165019:1–165019:20.
17. Kostelecký, V.A.; Russellb, N. Data Tables for Lorentz and CPT Violation. *Rev. Modern Phys.* **2017**, *83*, 11.
18. Bailey, Q.G. Time Delay and Doppler Tests of the Lorentz Symmetry of Gravity. *Phys. Rev.* **2009**, *D80*, 044004:1–022006:13.
19. Kostelecký, V.A.; Tasson, J.D. Prospects for Large Relativity Violations in Matter-Gravity Couplings. *Phys. Rev. Lett.* **2009**, *102*, 010402:1–010402:4.
20. Komatsu, E.; Smith, K.M.; Dunkley, J.; Bennett, C.L.; Gold, B.; Hinshaw, G.; Jarosik, N.; Larson, D.; Nolta, M.R.; Page, L.; et al. Seven-Year Wilkinson Microwave Anisotropy Probe(WMAP) Observations: Cosmological Interpretation. *Astrophys. J. Suppl.* **2011**, *192*, 18:1–18:47.
21. Muller,H.; Chiow, S.; Herrmann, S.; Chu, S.; Chung, K.Y. Atom-Interferometry Tests of the Isotropy of Post-Newtonian Gravity. *Phys. Rev. Lett.* **2008**, *100*, 031101:1–031101:4.
22. Bourgoin, A.; Hees, A.; Bouquillon, S.; LePoncin-Lafitte, C.; Francou, G.; Angonin, M.C. Testing Lorentz symmetry with Lunar Laser Ranging. *Phys. Rev. Lett.* **2016**, *117*, 241301:1–241301:6.
23. Kostelecký, V.A.; Tasson , J.D. Constraints on Lorentz Violation from Gravitational Č Erenkov Radiation. *Phys. Lett. B* **2015**, *749*, 551–559.
24. Shao, L.J. Tests of Local Lorentz Invariance Violation of Gravity in the Standard Model Extension with Pulsars. *Phys. Rev. Lett.* **2014**, *112*, 111103:1–111103:5.
25. Shao, C.G.; Tan, Y.J.; Tan, W.H.; Yang, S.Q.; Luo, J.; Tobar, M.E.; Bailey, Q.G.; Long, J.C.; Weisman, E.; Xu, R.; et al. Combined Search for Lorentz Violation in Short-Range Gravity. *Phys. Rev. Lett.* **2016**, *117*, 071102:1–071102:6.
26. Yang, S.Q.; Zhan, B.F.; Wang, Q.L.; Shao, C.G.; Tu, L.C.; Tan, W.H.; Luo, J. Test of the Gravitational Inverse Square Law at Millimeter Ranges. *Phys. Rev. Lett.* **2012**, *108*, 081101:1–081101:8.
27. Tan, W.H.; Yang, S.Q.; Shao, C.G.; Li, J.; Du, A.B.; Zhan, B.F.; Wang, Q.L.; Luo, P.S.; Tu, L.C.; Luo, J. New Test of the Gravitational Inverse-Square Law at the Submillimeter Range with Dual Modulation and Compensation. *Phys. Rev. Lett.* **2016**, *116*, 131101:1–131101:5.
28. Long, J.C.; Kostelecký, V.A. Search for Lorentz Violation in Short-Range Gravity. *Phys. Rev. D* **2015**, *91*, 092003:1–092003:6.
29. Shao, C.G.; Chen, Y.F.; Tan, Y.J.; Luo, J.; Yang, S.Q. Enhanced Sensitivity to Lorentz Invariance Violations in Short-Range Gravity Experiments. *Phys. Rev. D* **2016**, *94*, 104061:1–104061:12.
30. Bailey, Q.G.; Kostelecký, V.A.; Xu, R. Short-Range Gravity and Lorentz Violation. *Phys. Rev. D* **2015**, *91*, 022006:1–022006:6.
31. Colladay, D.; Kostelecký, V.A. CPT Violation and the Standard Model. *Phys. Rev. D* **1997**, *55*, 6760–6774.
32. Colladay, D.; Kostelecký, V.A. Lorentz-violating extension of the standard model. *Phys. Rev. D* **1998**, *58*, 116002:1–116002:23.
33. Bluhm, R.; Kostelecký, V.A.; Lane, C.D.; Russell, N. Probing Lorentz and CPT violation with space-based experiments. *Phys. Rev. D* **2003**, *68*, 125008:1–125008:14.
34. Bluhm, R.; Kostelecký, V.A.; Lane, C.D.; Russell, N. Clock-Comparison Tests of Lorentz and CPT Symmetry in Space. *Phys. Rev. Lett.* **2002**, *88*, 090801:1–090801:4.
35. Kostelecký, V.A.; Mewes, M. Signals for Lorentz Violation in Electrodynamics. *Phys. Rev. D* **2002**, *66*, 056005:1–056005:24.
36. Kostelecký, V.A. Sensitivity of CPT Tests with Neutral Mesons. *Phys. Rev. Lett.* **1998**, *80*, 1818:1–1818:4.

37. Kostelecký, V.A.; Mewes, W. Testing Local Lorentz Invariance with Short-Range Gravity. *Phys. Lett. B* **2017**, *766*, 137–143.
38. Shao, C.G.; Tan, Y.J.; Tan, W.H.; Yang, S.Q.; Luo, J.; Tobar, M.E. Search for Lorentz Invariance Violation through Tests of the Gravitational Inverse Square Law at Short Ranges. *Phys. Rev. D* **2015**, *91*, 102007:1–102007:5.